



# Space-variant video compression and processing in digital holographic microscopy sensor networks with application to potable water monitoring

TOMI PITKÄAHO,<sup>1,5</sup> VILLE PITKÄKANGAS,<sup>2</sup>  MIKKO NIEMELÄ,<sup>2</sup> SUDHEESH K. RAJPUT,<sup>3,4</sup> NAVEEN K. NISHCHAL,<sup>3</sup> AND THOMAS J. NAUGHTON<sup>1,6</sup>

<sup>1</sup>Department of Computer Science, Maynooth University–National University of Ireland Maynooth, Maynooth, County Kildare, Ireland

<sup>2</sup>University of Oulu, Oulu Southern Institute, Pajatie 5, 85500 Nivala, Finland

<sup>3</sup>Department of Physics, Indian Institute of Technology Patna Bihta, Patna 801 103, India

<sup>4</sup>Department of Systems Science, Graduate School of System Informatics Kobe University, Rokkodai 1-1 Nada, Kobe 657-8501, Japan

<sup>5</sup>e-mail: tomi.pitkaaho@mu.ie

<sup>6</sup>e-mail: tomn@cs.nuim.ie

Received 3 April 2018; revised 3 July 2018; accepted 4 July 2018; posted 5 July 2018 (Doc. ID 327476); published 27 July 2018

Water-related diseases affect societies in all parts of the world. Online sensors are considered a solution to the problems associated with laboratory testing in potable water. One of the most active research areas of such online sensors has been within optics. Digital holographic microscopy (DHM) has the potential to rival state-of-the-art techniques such as advanced turbidity measurement. However, its use as an online sensor is limited by the large data requirements typical for digital holographic video. In this paper, we provide a solution that permits DHM to be applied to a whole class of online remote sensor networks, of which potable water analysis is one example. The designed sensors incorporate a novel space-variant quantization algorithm to preprocess each frame of a video sequence before transmission over a network. The system satisfies the generally accepted requirements of an online system: automated, near real-time, and operating in a real environment. To verify the effectiveness of the design, we implemented and evaluated it in an active potable water facility. © 2018 Optical Society of America

**OCIS codes:** (090.1995) Digital holography; (100.6890) Three-dimensional image processing; (180.6900) Three-dimensional microscopy.

<https://doi.org/10.1364/AO.57.00E190>

## 1. INTRODUCTION

Water-related diseases (WRDs), such as diarrhea, typhoid fever, and hepatitis A, remain one class of major global health concerns [1]. Nearly 90% of diarrheal diseases are caused by poor-quality drinking and bathing water [2]. According to the World Health Organization (WHO), globally 10% of all deaths among children under five are caused by diarrhea [3]. As the water is usually distributed to a large number of consumers from the same source, in the case of contamination at a single location, widespread infection is possible.

The microbiological quality of drinking water, regulated by governmental bodies, is determined typically by onsite water sampling followed by transportation to a laboratory where the actual analysis is performed. This procedure has two major problems. First, as the sampling is done at intervals, each sample represents only a fraction of the total water going through the system, such as a water pumping station. Changes in the

water's microbiological quality can occur between the sample gatherings. The second major problem is the delay between gathering the sample and obtaining the result from analysis. As the microbiological quality is determined by culturing the sample in the laboratory, the delay can be more than 18 h. Both of these problems pose risks to public health.

To increase safety and to ensure high microbiological quality of potable water, the use of online sensors has been suggested [4,5]. In the context of this work, we define an online sensor as one that (i) has a higher (close to real-time) response time and higher sampling frequency than laboratory-based methods, (ii) has a comparable reliability to laboratory-based methods in terms of few false positives and false negatives, and (iii) has highly accessible results (e.g., should permit Internet access if at a remote location).

Of the optical sensors employed in this field [5–10], sensors measuring turbidity are among the most popular. Turbidity

measurement can be considered as an indirect measurement of microbiological water quality, but it cannot differentiate between organic and inorganic particles. One of the most sophisticated forms of turbidity measurement is multiangle light-scattering (MALS) measurement, which captures light at several angles of refraction [6,11]. Unfortunately, MALS is limited to a single object in its field of view, requires precise alignment between the source and the sensor, and works only on relatively small volumes. Spectroscopy, such as Raman spectroscopy [7], Fourier-transform infrared spectroscopy [8], ultraviolet-visible spectroscopy [9], and fluorescence spectroscopy [10] have also been reported in water quality research. However, spectroscopic methods, too, are typically limited to small sample volumes that limit their sampling rate.

### A. Anticipated Advantages of DHM

Digital holographic microscopy (DHM) is an imaging technique that is well suited for real-time imaging of three-dimensional (3D) objects [12–30]. Digital holography can be regarded as an enhancement of light-scattering approaches with the following desirable properties: (i) the scattering from the object is captured holographically so that the scattering can be reversed in software, thus generating an in-focus image of the object at any distance from the camera, (ii) a relatively large volume can be imaged so that the object does not have to be in any special location, and (iii) multiple objects can be imaged (sensed) and recognized (distinguished) simultaneously.

These properties have the potential to provide advantages over MALS. One implication of property (i) is that any employed database of morphological scattering signatures can be simplified compared with MALS. By this, we mean that rather than compiling a set of scattering signatures for each object type and for each scattering distance for MALS, with DHM one needs only to store a signature for the in-focus object shape directly, because in software one can propagate from the hologram to the in-focus object for any scattering distance. Another implication of property (i) is that multiple joined objects can be distinguished with DHM, whereas with MALS they would generate a scattering pattern that is so difficult to analyze that most MALS implementations insist on only one object at a time being in the scattering beam. We propose that both of these implications would give rise to a lower false positive rate, which is a common problem with light-scattering approaches [5].

Two implications of property (ii) are that alignment issues between the scattering beam and the sample are relaxed, and that a larger range of object sizes can be accommodated. An implication of property (iii) is that higher throughputs should be possible.

### B. Major Obstacle to Use of DHM in Sensor Networks

The major obstacle to an online and remote DHM system for water quality measurement currently is the data requirements of digital holographic video, which are large with respect to the small number of pixels in the final imaged particle. Also, the low frequency of particles typically in potable water means that many holograms without a sensed particle may be transmitted unnecessarily. The data requirements are a critical consideration because network bandwidth is usually the primary bottleneck in achieving a high sampling density with online sensors.

Due to their high noise content, digital holograms have been shown to yield relatively modest results in general-purpose data-compression studies [31].

We propose that this obstacle to DHM's widespread use in remote online systems can be overcome by carefully partitioning the hologram image processing and analysis within the system and designing a special-purpose video compression scheme. We argue that a special-purpose hologram video compression algorithm is warranted because of the unique *a priori* knowledge one has of the sensed objects in DHM sensor networks.

The rest of the paper is organized as follows: in Section 2 the identified design choices are described; in Section 3, the developed compression algorithm is introduced; in Section 4, an implementation of the system is described; and Section 5 concludes the work.

## 2. DESIGN CHOICES

We identify four major design choices for such an online system: (A) optical hardware and architecture, (B) location of data processing and analyses, (C) processing and analysis algorithms, and (D) hologram video compression.

### A. Optical Hardware and Architecture

A typical sensor network consists of data measurement nodes and a gateway that enables users to access the data (Fig. 1). Here, the measurement node contains a DHM sensor. The trade-offs between various interferometer architectures and illumination choices have been well studied [13,21,29]. For example, a free-space propagation DHM [21,32] avoids the need for an expensive microscope objective, but suffers from a depth-dependent spatial resolution and vibration-sensitive alignment of a pinhole to produce the spherical wave.

### B. Location of Data Processing and Analyses

Due to the large volume of data in holographic video of real-world objects, networked holographic video applications have an ever-present problem of how to optimally partition the data processing between the capture side (before network transmission) and the display side [33,34], as illustrated in Fig. 1. For each application, the conclusion can be different. Data processing and analysis choices directly affect overall system capabilities, as summarized in Table 1. At one extreme,

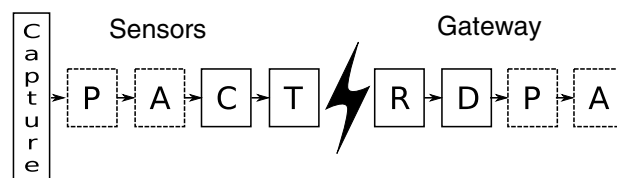


**Fig. 1.** DHM sensor network and design choices. A plurality of holographic sensors transmits holographic data over a network to a gateway. Design choices for where to conduct hologram image processing and analysis in a DHM sensor network. P, process; A, analyze; C, compress; T, transmit; R, receive; D, decompress. At one extreme, all data processing and analysis are conducted at the measurement node only, and minimal data are compressed and transmitted to the gateway. At the other extreme, raw hologram data are compressed at the measurement node and transmitted to the gateway, where all processing and analysis takes place. Table 1 summarizes the trade-off.

**Table 1. Primary Disadvantage of Each Simple Design Choice When Partitioning the Data Processing between Measurement Nodes (before Network Transmission) and Gateway**

	Measurement Node (Low Processing Power)	Measurement Node (High Processing Power)
Gateway (low processing power)	Not applicable—insufficient computing capabilities in overall system to analyze data	Not possible to perform inexpensive software upgrade of system functionality because gateway's computational resources are too restrictive
Gateway (high processing power)	Low temporal sampling density because of high network bandwidth requirements	Expensive to deploy and upgrade hardware; less reliable in harsh environments

the measurement node can be a simple low-calculation-power device that records, compresses, and transmits raw holographic video, with all computationally expensive processing and analysis tasks performed at the gateway. This approach has the major disadvantage that it requires significant network bandwidth and thus imposes a limit on the water sampling density possible with the system.

Alternatively, at the other extreme, all processing and analysis could be performed at the measurement node, and the gateway could be a simple device, requiring very little network bandwidth. This approach has the major disadvantages that it is difficult to upgrade the system for higher throughputs because many individual measurement nodes would need to be upgraded, and having many sophisticated measurement nodes would drive up costs (in terms of initial outlay and reliability in

harsh environments due to mechanical cooling measures, for example).

Our proposal is to carefully partition the data processing and analysis between measurement nodes and gateway. The major disadvantages of each approach could be avoided, without sacrificing either one's advantages. The challenge is to find algorithms for the measurement nodes that are:

1. effective: measurement node algorithms must be effective at preprocessing and compressing the hologram video data such that network bandwidth requirements are low (compared to transmitting the raw video data) and water temporal sampling density is high, and
2. efficient: at the same time, the measurement node algorithms need to be computationally simple and efficient such that the computer has sufficiently modest computing hardware

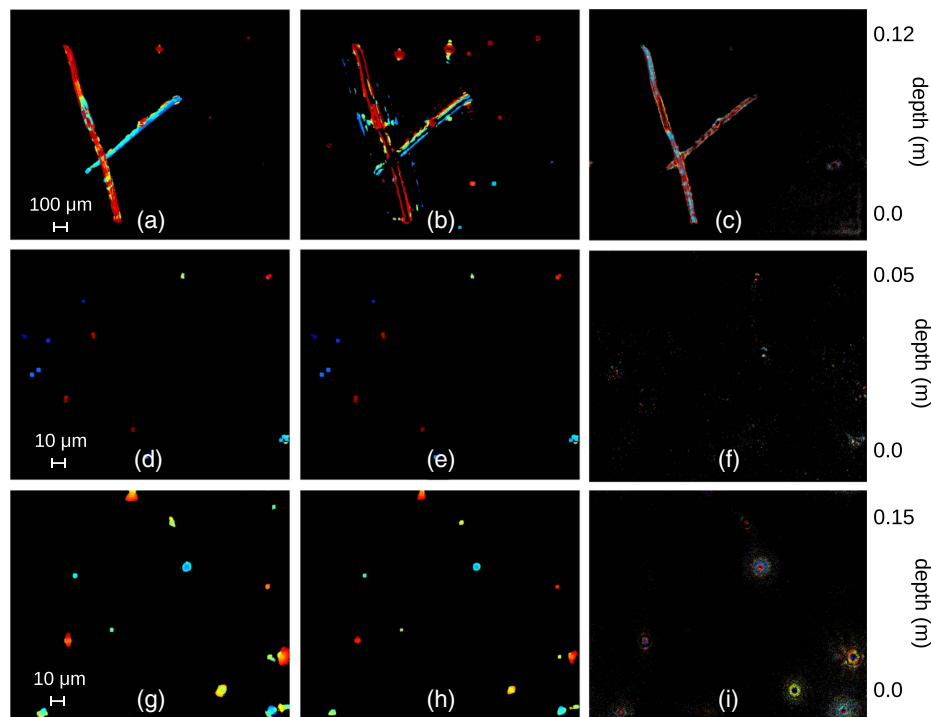


**Fig. 2.** Comparison of three DHM object localization techniques applied to each of three different classes of sample (top row, semitransparent rayon fibers; middle row, living *E. coli* bacteria; bottom row, 1  $\mu\text{m}$  latex beads). The three techniques were (a), (d), (g) Tamura contrast coefficient; (b), (e), (h) variance; (c), (f), (i) amplitude. The Tamura contrast coefficient approximation [38] is calculated for each pixel on each layer of the inverted amplitude reconstruction volume by using blockwise processing [37]. Variance and amplitude are calculated in the same manner. Color coding is used for depth. The rayon fibers were captured with the setup described in Ref. [37] and the other two as described in Section 4 of this paper. Tamura contrast and variance work well for *E. coli* and latex beads; however, variance identifies only the edges of the rayon fibers. Amplitude analysis, in general and for these samples also, identifies the lateral positions but fails in the identification of axial positions.

requirements. A simple measurement node is more reliable, more robust, and more cost-effective.

3. minimal: the computationally expensive processing should be performed at the gateway, so there will be no need to upgrade the measurement nodes (in terms of software or hardware) when upgrading the most sophisticated data-processing algorithms in the system. Reliable, over-the-air software upgrade of remote measurement nodes can be possible with a good framework design, but this is still a difficult problem in the general case [35].

**C. Processing and Analyses Algorithms**

As the system is required to be near-real-time, algorithms need to be optimized and chosen on the basis of the specific application. In the literature, objects have been found in hologram reconstruction volumes using amplitude analysis [27], edge detection [36], and contrast analysis [37]. However, as shown in Fig. 2, a different set of methods is appropriate for each application.

**D. Hologram Video Compression**

Hologram video compression is necessary because, in practice, the limiting factor on the sampling density of the system is the data throughput over the network. The most general algorithms do not presuppose any particular type of hologram data and so yield modest compression results [31]. However, we propose that in DHM sensor networks, the objects sensed are from such a restricted class, and known *a priori*, that we can do much better than the tools created for general-purpose digital hologram compression. In the next section, we introduce a novel compression technique that is specific to DHM sensor network applications.

**3. COMPRESSION**

The principle employed in this compression strategy is to partition (temporally and spatially) the regions of pixels in the hologram video sequence according to how much information they contain about the sensed particles, and represent those regions with a number of bits per pixel proportional to how much information they contain. It is called space-variant compression because the number of quantization levels per pixel is dependent on that pixel’s spatial location in the hologram domain. Space-variant quantization has similarities to nonuniform digital hologram quantization [39,40] but is distinct because in that work Shortt *et al.* determined the number of quantization levels to employ based on the hologram pixels’ complex values and ignored their spatial locations. Our approach is complementary to the ongoing efforts in compressive sensing of digital holograms [41,42]. However, our space-variant quantization can be regarded as a subtle enhancement of compressive sensing schemes where pixels are either included or not included (as is the case of [42], for example) because here we include pixels with varying numbers of bits of representation (including the possibility of zero bits).

The approach is as follows. Starting from the second hologram in the video sequence, and for each hologram, we apply the steps as shown in Fig. 3. Holograms are subtracted from their predecessor to generate a subtraction hologram. This can increase the reconstruction quality by removing the effects

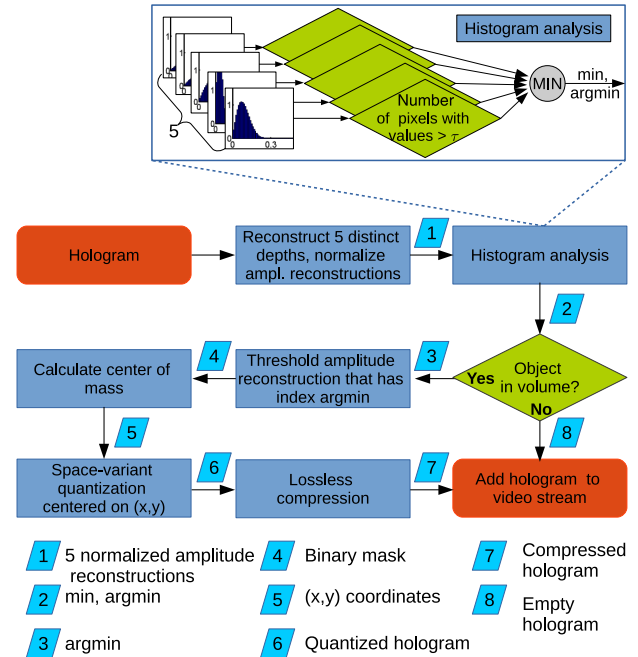


**Fig. 3.** Data compression pipeline for each frame in the hologram video sequence. The input for the compression algorithm is a subtraction hologram, and the output is a compressed hologram. The inset illustrates how the histogram analysis is executed. Each number 1 through 8 denotes the data type at that point in the pipeline.

of impurities and unwanted reflections [21] and increase compression ratio by removing noise.

A fixed number of intensity images is reconstructed from the subtraction hologram, with a predefined depth interval, and analyzed efficiently based on their histograms for the presence of a particle. Using a typical hologram in each case, Fig. 4 shows that reconstructions with and without near in-focus objects

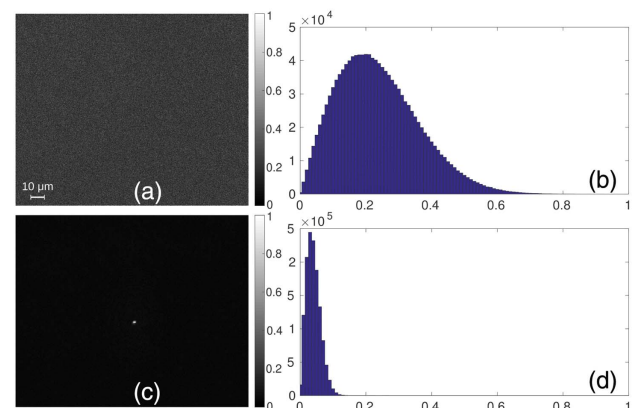


**Fig. 4.** Illustration of the inputs to histogram analysis (using a hologram from the application described later in the paper). (a), (b) Intensity reconstruction at -150 mm from a hologram without an object and its histogram, respectively; (c), (d) intensity reconstruction at -150 mm from a hologram with an object and its histogram, respectively.

have distinct histograms. If the number of pixels with intensity values higher than intensity threshold  $\tau$  is less than a predefined threshold  $\gamma$ , then that reconstruction is assumed to contain a near in-focus object. The threshold values  $\tau$  and  $\gamma$ , and the reconstruction depth interval, must be chosen experimentally based on one's application. By keeping the depth of sample volume narrow enough, a relatively small number of reconstructions can be used for a reliable detection of objects' presence, as the objects do not have to be fully in focus. Alternatively, one can increase the number of reconstructions with a cost of higher processing time.

If it is determined that the subtraction hologram does not contain a particle, that whole frame of the hologram video sequence is replaced with a placeholder (an empty hologram) that requires only a few bytes to represent (data type 8 in Fig. 3). If it is determined that the subtraction hologram contains a particle, the reconstruction at the depth closest to the particle is binarized by thresholding to determine the object's center of mass (item 5 in Fig. 3). These exact coordinates are used to partition the subtraction hologram into concentric circular regions, centered on the axial position of the particle, so that it can be quantized using different numbers of quantization levels (see Fig. 5). By knowing the point spread function (PSF) of the system, the object-to-camera-distance, and the estimated lateral size of the object, one can define an appropriate sequence of diameters for one's application. If a single field of view contains multiple objects, overlapping areas of the concentric regions  $\beta_1$ ,  $\beta_2$ , and  $\beta_3$  around each object adopt the highest number of bits determined for any  $\beta$ .

Each space-variant quantization option is characterized by a pair of triples  $(\beta_1, \beta_2, \beta_3) \in \mathbb{R}^3$  and  $(b_1, b_2, b_3) \in \mathbb{N}^3$ , where  $b_1 \geq b_2 \geq b_3$ . Each  $\beta_i$  defines the diameter of one concentric circle, and the corresponding  $b_i$  defines the number of bits with which to quantize each pixel in that region. A lower  $b_i$  value results in lower data requirements for each holographic pixel and lower amplitude quality in the resulting reconstruction. For each application, an appropriate trade-off should be found experimentally between quantization and reconstruction quality. In addition, it is possible to use any number of regions and different shapes for regions.

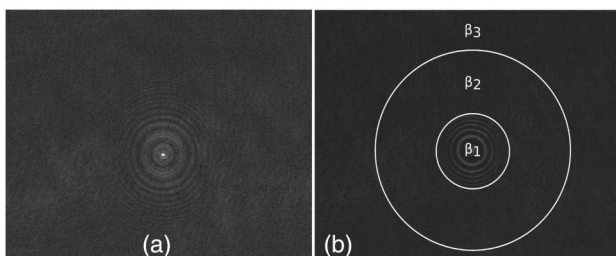


**Fig. 5.** Illustration of space-variant hologram quantization (using a hologram from the application described later in the paper). (a) Amplitude reconstruction at  $-140$  mm from the hologram plane with an object in focus, hologram size  $1280$  pixels  $\times$   $1024$  pixels; (b) hologram partitioned into three concentric regions to which varying amounts of quantization are applied (pixels in region  $\beta_1$  are allowed more quantization levels than in region  $\beta_2$ , and so on). The object need not be centered on the optical axis as in this example.

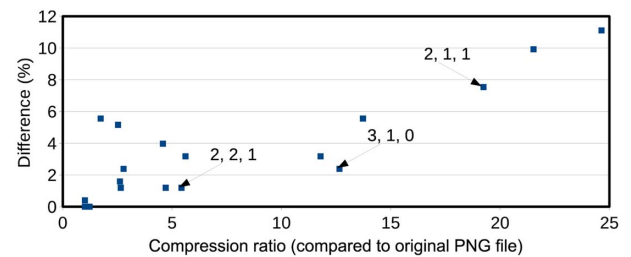


**Fig. 6.** Trade-off between compression ratio and reconstruction quality, for various values of  $(b_1, b_2, b_3)$ , using the hologram and  $\beta_i$  values from Fig. 5. A higher compression ratio is better. A lower percentage difference is better. The choice is determined by the minimum quality required by one's processing and analysis algorithms.

A particular value for  $(b_1, b_2, b_3)$  was evaluated using two parameters as follows. Space-variant quantization was applied to an original unquantized hologram  $H$  to yield  $H'$  that was losslessly compressed using the portable network graphics (PNG) standard [43]. PNG uses the LZ77 algorithm and Huffman coding. The compressed size in bytes of  $H'$  was divided into the size of  $H$ , similarly losslessly compressed with PNG, resulting in a value called the compression ratio. For the second parameter, the binary segmentation mask obtained by using the Tamura coefficient of the reconstructed amplitude from  $H'$  was compared (normalized sum of absolute differences) with an equivalently obtained mask using the reconstruction from  $H$ . Both parameters are plotted for various values of  $(b_1, b_2, b_3)$  in Fig. 6.

As the simplest option, we have chosen intensity quantization in the hologram domain as the lossy component of our compression strategy. However, any state-of-the-art lossy compression scheme can be adapted to the space-variant strategy proposed in this paper, and comparison of several of these could be the subject of a separate study.

#### 4. IMPLEMENTATION

To verify the effectiveness of the design, a physical implementation using inexpensive off-the-shelf components was built and evaluated in an active potable water facility. The imaging sensor was an inline DHM, illustrated in Fig. 7, whose principal components were a 405 nm laser module (CNI PGL-D8-405-50), a flow-through channel (Ibidi, 81121  $\mu$ -Slide 0.1 Luer), a 40X microscope objective (Olympus PLN 40X), and a  $1280 \times 1024$  pixel complementary metal oxide semiconductor camera with  $5.3$   $\mu$ m pixel pitch (IDS Imaging UI-1242LE-M). The remote sensor unit included a fanless computer [Thinclient Zotac Zbox, ZOTAC International (MCO) Ltd., Macao, Hong Kong], and the gateway was a custom-built personal computer that used a graphics card for digital hologram processing [44]. The fanless computer was capable of performing one full-resolution reconstruction approximately in 1 s.

The sensor was evaluated in a laboratory environment with various test objects. A static 1951 USAF resolution test chart was imaged before incorporating the flow-through channel and water circulation system. In addition, the system was tested with moving  $1$   $\mu$ m latex beads. These resolution tests are shown

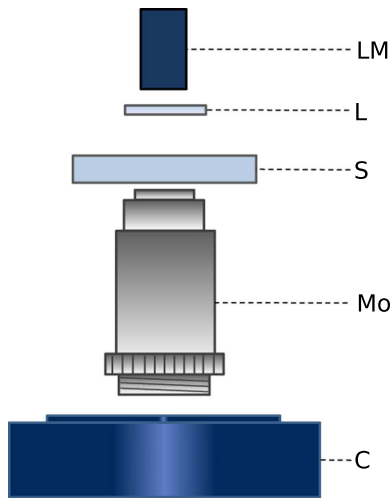


**Fig. 7.** Imaging sensor components. Light from the laser module (LM) is collimated by the lens (L) and transmitted through an aperture containing the sample (S). Magnification is realized with the microscope objective (MO), and the hologram is captured with the digital camera (C).

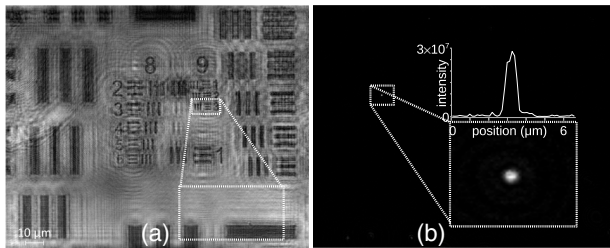


**Fig. 8.** Resolution test. (a) USAF 1951 resolution chart. The linewidth of the smallest element is 780 nm (element 3 of group 9 in inset). (b) 1  $\mu\text{m}$  latex beads in waterflow. Estimated flow speed of 4 ml/min was controlled by a peristaltic pump (Welco WPM1). The inset shows magnified intensity of one latex bead at  $-48$  mm from the hologram plane together with a horizontal intensity profile going through the center of the object.

in Fig. 8; it can be verified that the resolution of the system is suitable for imaging objects smaller than 1  $\mu\text{m}$ .

After adding the flow-through channel, the system was tested using living *Escherichia coli* (*E. coli*). *E. coli* was chosen, as it is the most commonly used bacterial indicator for a fecal pollution [45,46]. Cultured living *E. coli* was collected from a Petri dish with an inoculation needle and mixed with 100 ml of sterile water. The mixture was manually pushed through the flow-through channel, and digital holograms were captured at the maximum frame rate of the camera with the full resolution (Fig. 9).

For tests in an active potable water facility, a portable version of the sensor was assembled in a commercially available aluminum case that contained a low-calculating-power computer unit, the imaging and sample circulation components as described above, and a 3G modem (Huawei E367). The flow

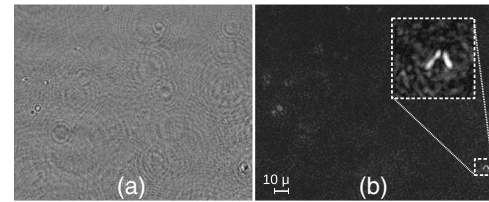


**Fig. 9.** Result with *E. coli*. (a) Subtraction hologram; (b) intensity reconstruction at  $-17.1$  mm from the hologram. The white rectangle in (b) shows a region where a single *E. coli* was identified. The bacterium appears twice, as the water flow was slow enough for the object to be imaged in both frames of the subtraction hologram (magnified in inset).

speed was controlled with a variable area flow meter (Kytola Instruments Inc.). This flow-through channel with 100  $\mu\text{m}$  depth and variable area flow meter together prevented turbulence that might cause some particles to be imaged multiple times. In object detection (as part of the compression algorithm), holograms were reconstructed at five distinct depths with 25  $\mu\text{m}$  intervals starting from the front plane of the flow-through channel. The compression algorithm parameters  $\gamma$  and  $\tau$  were  $10^4$  and 0.3, respectively.

The Finnish wholesale potable water company Vesikolmio Oy (Nivala, Finland, [www.vesikolmio.fi](http://www.vesikolmio.fi)), which serves water to 50,000 people and annually delivers 3.7 million  $\text{m}^3$  of water, provided access to one of their ground-water pumping stations. The system was installed before the ultraviolet water purification system for a testing period of two months. During the two-month testing period, the system was capable of capturing multiple holograms that contained microparticles (example shown in Fig. 10). There were no water-contamination issues during the test period, and no biological contaminants were found in the water supply. For a quantification of the performance of the system in a laboratory setting, a reservoir of contaminated water should be used. The purpose of the onsite testing at the pumping station was to demonstrate deployment possibilities. For further consideration at remote sites, the parameters of a proposed algorithm should have performance bounds and values that have been validated in real settings. This is future work.

#### A. Automated Image Processing and Analysis

In order to image process and analyze these holograms, an automated procedure was developed. The objects were localized

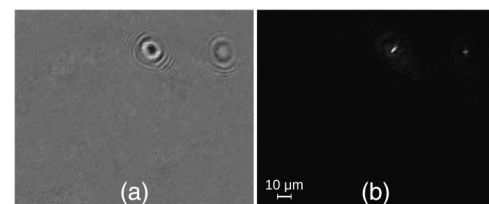


**Fig. 10.** Typical result from the active potable water facility. (a) Subtraction hologram; (b) intensity reconstruction at  $-159$  mm from the hologram plane, where a single microscopic object is in focus.

and segmented using Tamura coefficient approximation [37]. The 3D blobs (regions) were classified according to their morphology by calculating their eccentricity [29], as

$$\epsilon = \left[ 1 - \left( \frac{b}{a} \right)^2 \right]^{\frac{1}{2}}, \quad (1)$$

where  $a$  and  $b$  are the lengths of its longest and second longest orthogonal dimensions in 3D space, as calculated using principal component analysis (PCA). Eccentricity can be used to differentiate rod-shaped (such as bacilli) and spherical (such

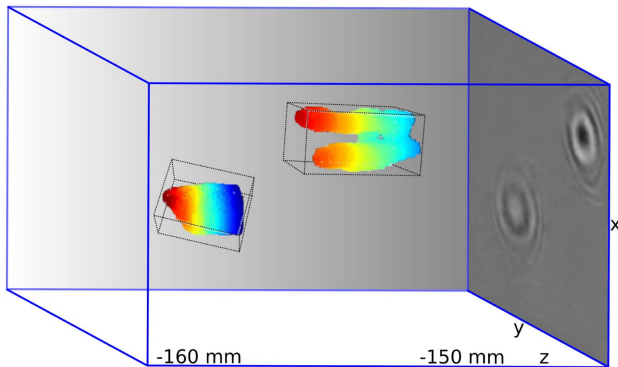


**Fig. 11.** Typical result from the active potable water facility with a hologram containing two microparticles. The 3D blobs are localized and segmented in the reconstruction volume, and the orientations of the bounding boxes found using PCA. Eccentricities of 0.63 and 0.78 were found for the upper and lower 3D blobs, respectively. Colors represent relative depth of particles.

as cocci) bacteria. A typical result with a hologram containing two microscopic objects is shown in Fig. 11. Another example with more detailed analysis is shown in Fig. 12. In these examples, the analysis was performed on the raw uncompressed holograms to allow us to appropriately choose the lossy compression parameters for the subsequent study.

## 5. CONCLUSION

The use of DHM as an online sensor in a sensor network is limited by the large data requirements typical for digital holographic video. In this paper, we provided a solution that permits DHM to be applied to a whole class of online remote sensor networks, of which potable water analysis is one example explored in detail. The solution consists of a software framework to handle the holographic data from its capture, through its processing, to its analysis. We demonstrated the unique *a priori* knowledge one would have in DHM sensor networks of this type, and how that motivates a novel space-variant digital holographic video quantization algorithm. The efficient reduction in data, without sacrificing accuracy, allows DHM sensor networks of this type to satisfy the generally accepted requirements of an online system: automated, near real-time, and operating in a real environment. To verify the effectiveness of the design, a physical implementation using inexpensive off-the-shelf components was built and evaluated in an active potable water facility. Our conclusion is that DHM now has the potential to rival state-of-the-art techniques such as advanced turbidity measurement. Broader applications include the search for microbial life in extreme environments [47].

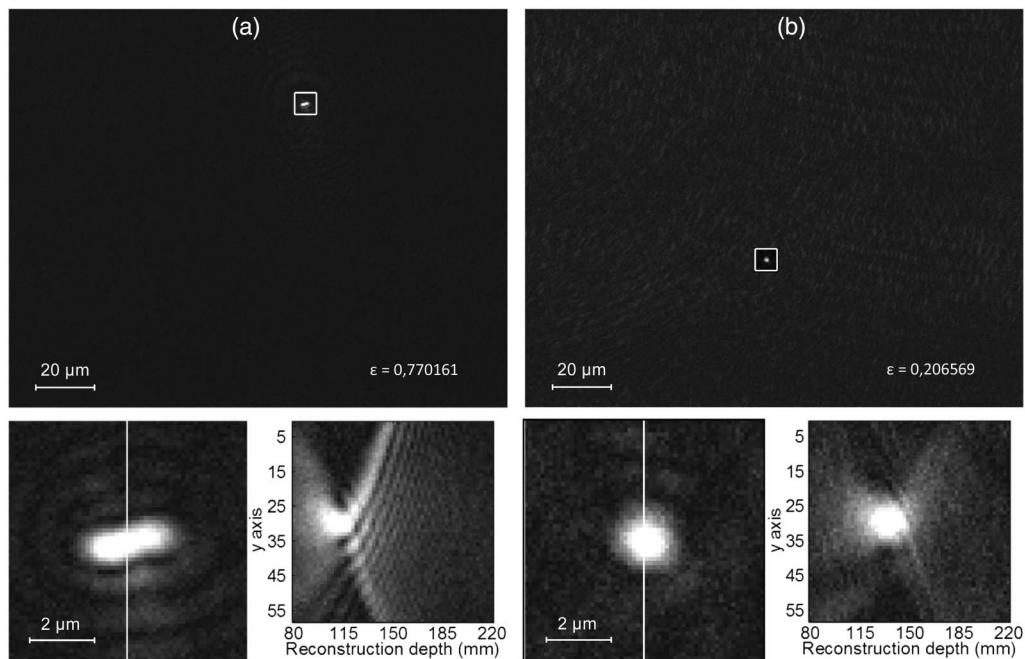


**Fig. 12.** Typical results from the active potable water facility. The first row shows intensity reconstructions at full size (with a white rectangle indicating the identified object), bottom row shows the magnified object, and a  $y$ - $z$  intensity plane (side profile) through the volume along the white vertical line in the magnified object. (a) Reconstruction depth 113 mm, object size  $2.84 \mu\text{m} \times 1.81 \mu\text{m} \times 0.77 \mu\text{m}$ ; (b) reconstruction depth 131 mm, object size  $2.21 \mu\text{m} \times 2.16 \mu\text{m} \times 1.2 \mu\text{m}$ .  $\epsilon$  denotes eccentricity.

**Funding.** Science Foundation Ireland (SFI) (13/CDA/2224); Irish Research Council; European Regional Development Fund (ERDF) (Council of Oulu Region project no. A31655); Maud Kuistilan Muistosäätiö; Kerttu Saalasti Säätiö.

**Acknowledgment.** The authors thank Vesikolmio Oy, Nivala, Finland for providing access to their potable water facility.

## REFERENCES

- WHO, "Progress and challenges on water and health: the role of the protocol on water and health," Technical Report EUR/55934/BD/3 (World Health Organization, 2010).
- WHO, "Water, sanitation and hygiene links to health facts and figures," Technical Report (World Health Organization, 2004). Accessed from <http://www.who.int/iris/handle/10665/69489>.
- WHO, "World health statistics 2013," Technical Report (World Health Organization, 2013).
- M. V. Storey, B. van der Gaag, and B. P. Burns, "Advances in on-line drinking water quality monitoring and early warning systems," *Water Res.* **45**, 741–747 (2011).
- R. Lopez-Roldan, P. Tusell, S. Courtois, and J. L. Cortina, "On-line bacteriological detection in water," *TrAC Trends Anal. Chem.* **44**, 46–57 (2013).
- P. J. Wyatt, "Differential light scattering: a physical method for identifying living bacterial cells," *Appl. Opt.* **7**, 1879–1896 (1968).
- A. Sengupta, M. Mujacic, and E. J. Davis, "Detection of bacteria by surface-enhanced Raman spectroscopy," *Anal. Bioanal. Chem.* **386**, 1379–1386 (2006).
- C. Yu, J. Irudayaraj, C. Debroy, Z. Schmilovitch, and A. Mizrach, "Spectroscopic differentiation and quantification of microorganisms in apple juice," *J. Food Sci.* **69**, 268–272 (2004).
- J. van den Broeke, P. Ross, A. V. der Helm, E. Baars, and L. C. Rietveld, "Use of on-line UV/Vis-spectrometry in the measurement of dissolved ozone and AOC concentrations in drinking water treatment," *Water Sci. Technol.* **57**, 1169–1175 (2008).
- R. K. Henderson, A. Baker, K. R. Murphy, A. Hambly, R. M. Stuetz, and S. J. Khan, "Fluorescence as a potential monitoring tool for recycled water systems: a review," *Water Res.* **43**, 863–881 (2009).
- P. J. Wyatt, "Identification of bacteria by differential light scattering," *Nature* **221**, 1257–1258 (1969).
- T. Zhang and I. Yamaguchi, "Three-dimensional microscopy with phase-shifting digital holography," *Opt. Lett.* **23**, 1221–1223 (1998).
- E. Cucho, F. Bevilacqua, and C. Depeursinge, "Digital holography for quantitative phase-contrast imaging," *Opt. Lett.* **24**, 291–293 (1999).
- F. Dubois, L. Joannes, and J.-C. Legros, "Improved three-dimensional imaging with a digital holography microscope with a source of partial spatial coherence," *Appl. Opt.* **38**, 7085–7094 (1999).
- S. Murata and N. Yasuda, "Potential of digital holography in particle measurement," *Opt. Laser Technol.* **32**, 567–574 (2000).
- I. Yamaguchi, J.-i. Kato, S. Ohta, and J. Mizuno, "Image formation in phase-shifting digital holography and applications to microscopy," *Appl. Opt.* **40**, 6177–6186 (2001).
- G. Pedrini and H. J. Tiziani, "Short-coherence digital microscopy by use of a lensless holographic imaging system," *Appl. Opt.* **41**, 4489–4496 (2002).
- P. Ferraro, G. Coppola, S. D. Nicola, A. Finizio, and G. Pierattini, "Digital holographic microscope with automatic focus tracking by detecting sample displacement in real time," *Opt. Lett.* **28**, 1257–1259 (2003).
- D. Carl, B. Kemper, G. Wernicke, and G. von Bally, "Parameter-optimized digital holographic microscope for high-resolution living-cell analysis," *Appl. Opt.* **43**, 6536–6544 (2004).
- B. Javidi, I. Moon, S. Yeom, and E. Carapezza, "Three-dimensional imaging and recognition of microorganism using single-exposure on-line (SEOL) digital holography," *Opt. Express* **13**, 4492–4506 (2005).
- J. Garcia-Sucerquia, W. Xu, S. K. Jericho, P. Klages, M. H. Jericho, and H. J. Kreuzer, "Digital in-line holographic microscopy," *Appl. Opt.* **45**, 836–850 (2006).
- J. Kühn, T. Colomb, F. Montfort, F. Charrière, Y. Emery, E. Cucho, P. Marquet, and C. Depeursinge, "Real-time dual-wavelength digital holographic microscopy with a single hologram acquisition," *Opt. Express* **15**, 7231–7242 (2007).
- B. Kemper and G. von Bally, "Digital holographic microscopy for live cell applications and technical inspection," *Appl. Opt.* **47**, A52–A61 (2008).
- B. Rappaz, E. Cano, T. Colomb, J. Kühn, C. Depeursinge, V. Simanis, P. J. Magistretti, and P. Marquet, "Noninvasive characterization of the fission yeast cell cycle by monitoring dry mass with digital holographic microscopy," *J. Biomed. Opt.* **14**, 034049 (2009).
- O. Mudanyali, C. Oztoprak, D. Tseng, A. Erlinger, and A. Ozcan, "Detection of waterborne parasites using field-portable and cost-effective lensfree microscopy," *Lab Chip* **10**, 2419–2423 (2010).
- M. Lee, O. Yaglidere, and A. Ozcan, "Field-portable reflection and transmission microscopy based on lensless holography," *Biomed. Opt. Express* **2**, 2721–2730 (2011).
- J. F. Restrepo and J. Garcia-Sucerquia, "Automatic three-dimensional tracking of particles with high-numerical-aperture digital lensless holographic microscopy," *Opt. Lett.* **37**, 752–754 (2012).
- N. Pavillon, J. Kühn, C. Moratal, P. Jourdain, C. Depeursinge, P. J. Magistretti, and P. Marquet, "Early cell death detection with digital holographic microscopy," *PLoS ONE* **7**, e30912 (2012).
- A. E. Mallahi, C. Minetti, and F. Dubois, "Automated three-dimensional detection and classification of living organisms using digital holographic microscopy with partial spatial coherent source: application to the monitoring of drinking water resources," *Appl. Opt.* **52**, A68–A80 (2013).
- L. Miccio, P. Memmolo, F. Merola, S. Fusco, V. Embrione, A. Paciello, M. Ventre, P. A. Nettii, and P. Ferraro, "Particle tracking by full-field complex wavefront subtraction in digital holography microscopy," *Lab Chip* **14**, 1129–1134 (2014).
- T. J. Naughton, Y. Frauel, B. Javidi, and E. Tajahuerce, "Compression of digital holograms for three-dimensional object reconstruction and recognition," *Appl. Opt.* **41**, 4124–4132 (2002).
- D. Gabor, "A new microscopic principle," *Nature* **161**, 777–778 (1948).
- T. J. Naughton, J. B. McDonald, and B. Javidi, "Efficient compression of Fresnel fields for Internet transmission of three-dimensional images," *Appl. Opt.* **42**, 4758–4764 (2003).
- M. Kujawinska, T. Kozacki, C. Falldorf, T. Meeser, B. M. Hennelly, P. Garbat, W. Zaperty, M. Niemelä, G. Finke, M. Kowiel, and T. Naughton, "Multiwavefront digital holographic television," *Opt. Express* **22**, 2324–2336 (2014).
- S. Brown and C. J. Sreenan, "Software updating in wireless sensor networks: a survey and lacunae," *J. Sens. Actuator Netw.* **2**, 717–760 (2013).
- M. Kempkes, E. Darakis, T. Khanam, A. Rajendran, V. Kariwala, M. Mazzotti, T. J. Naughton, and A. K. Asundi, "Three dimensional digital holographic profiling of micro-fibers," *Opt. Express* **17**, 2938–2943 (2009).
- T. Pitkääho, M. Niemelä, and V. Pitkääkangas, "Partially coherent digital in-line holographic microscopy in characterization of a microscopic target," *Appl. Opt.* **53**, 3233–3240 (2014).
- P. Memmolo, C. Distanto, M. Paturzo, A. Finizio, P. Ferraro, and B. Javidi, "Automatic focusing in digital holography and its application to stretched holograms," *Opt. Lett.* **36**, 1945–1947 (2011).
- A. E. Shortt, T. J. Naughton, and B. Javidi, "A companding approach for nonuniform quantization of digital holograms of three-dimensional objects," *Opt. Express* **14**, 5129–5134 (2006).
- A. E. Shortt, T. J. Naughton, and B. Javidi, "Histogram approaches for lossy compression of digital holograms of three-dimensional objects," *IEEE Trans. Image Process.* **16**, 1548–1556 (2007).
- D. J. Brady, K. Choi, D. L. Marks, R. Horisaki, and S. Lim, "Compressive holography," *Opt. Express* **17**, 13040–13049 (2009).
- Y. Rivenson, A. Stern, and B. Javidi, "Compressive Fresnel holography," *J. Display Technol.* **6**, 506–509 (2010).
- G. Roelofs, *PNG: The Definitive Guide* (O'Reilly & Associates, 1999).

44. L. Ahrenberg, A. J. Page, B. M. Hennelly, J. B. McDonald, and T. J. Naughton, "Using commodity graphics hardware for real-time digital hologram view-reconstruction," *J. Display Technol.* **5**, 111–119 (2009).
45. R. M. Chalmers, H. Aird, and F. J. Bolton, "Waterborne *Escherichia coli* O157," *J. Appl. Microbiol.* **88**, 124S–132S (2000).
46. P. Tallon, B. Magajna, C. Lofranco, and K. T. Leung, "Microbial indicators of faecal contamination in water: a current perspective," *Water Air Soil Pollut.* **166**, 139–166 (2005).
47. E. Serabyn, K. Liewer, C. Lindensmith, K. Wallace, and J. Nadeau, "Compact, lensless digital holographic microscope for remote microbiology," *Opt. Express* **24**, 28540–28548 (2016).